Active Transient Acousto-Structural Response Control of a Smart Cavity-Coupled Circular Plate System

Seyyed M. HASHEMINEJAD, Rezgar SHAKERI

Acoustics Research Laboratory
Center of Excellence in Experimental Solid Mechanics and Dynamics
School of Mechanical Engineering
Iran University of Science and Technology
Narmak, Tehran 16846-13114 Iran; e-mail: hashemi@iust.ac.ir

The transient vibroacoustic response suppression of a piezo-coupled sandwich circular plate backed by a rigid-walled cylindrical acoustic enclosure is investigated. Problem formulation is based on the linear acoustic wave theory, Kirchhoff thin plate model, fluid/structure compatibility relations, Rayleigh integra formula, and active damping control (ADC) strategy. Matlab's Genetic Algorithm (GA) is utilized to identify and optimize the feedback controller gain parameter based on a multi-objective performance index function. Durbin's numerical Laplace inversion scheme is then used to calculate the key acousto-structural response parameters due to a transverse impulsive shock force for selected cavity depths. Numerical simulations demonstrate satisfactory performance of adopted control methodology in effective suppression of panel displacement response and radiated external sound pressure for enclosures of shallow and moderate depths. Limiting cases are considered and accuracy of the proposed model is rigorously verified.

Keywords: sound radiation; structural-borne noise control; coupled multi-field problem; piezoelectric disc actuator; cylindrical enclosure; GA-tuned controller.

1. Introduction

Suppressing vibroacoustic response of an acoustic space coupled with a flexible boundary structure is an important noise control problem with a wide variety of engineering applications such as in vehicular/aircraft cabins, building structures, industrial machines, and civil/marine structures. The traditional passive treatments (e.g., viscoelastic damping materials (NASHIF *et al.*, 1985)) are typically inappropriate at low excitation frequencies. Furthermore, they can substantially increase total structural weight and are prone to disintegration under sever environmental and frequency variations. With recent developments in the smart material technology, active control tactics that employ secondary force inputs (FULLER, 1990) and/or smart piezoelectric materials (HASHEMINEJAD, KESHAVARZPOUR, 2013; HASHEMINEJAD, ALAEI-VARNOSFADERANI, 2012; HASHEMINEJAD, RABBANI, 2015) have provided a viable means to deal with this problem. In particular, numerous researchers have employed various control methodologies to actively suppress sound radiation from (transmission through) cavity-coupled flexible plates or panels in the past few decades. Among them, (PAN, HANSEN, 1991) utilized a point force actuator for active control of noise transmission through a thin simply-supported aluminum panel into a rectangular parallelepiped acoustic cavity. KOSHIGOE *et al.* (1993) proposed a fully coupled acoustic/plate interaction model for active control of noise transmission from an external source into a rectangular cavity using surface-mounted piezoelectric actuators. CHENG, NICOLAS (1992) followed a variational approach to develop a coupled acousto-elastic formulation for steady-state sound radiation from a point-driven elastically-supported flexible circular end-plate into a hard-walled cylindrical enclosure in an attempt to control noise in an airplane cabin. VEERAMANI, WERELY (1996) utilized piezo-actuators in the context of a hybrid passive/active damping system to control sound radiation from a composite sandwiched visco-elastic plate as the boundary of a three dimensional rectangular enclosure. BALACHANDRAN *et al.* (1996) used microphone sen-

sors and surface-bonded piezo-ceramic (PZT) actuator patches to investigate active feed-forward noise control within a three-dimensional rectangular cavity with a flexible wall. Niekerk, Tongue (1997) presented an active H_2-optimal control methodology that employ piezo-ceramic patch actuators to reduce the transient noise transmitted into a three-dimensional rectangular cavity through a flexible wall. Shields *et al.* (1998) developed a finite element model to control low-frequency sound radiation from a rectangular plate into an acoustic cavity using patches of active piezoelectric-damping composites (APDC). Ro, Baz (1999) developed an acoustic finite element model for effective sound radiation control of a vibrating aluminum rectangular plate coupled with an acoustic cavity by using active constrained layer damping (ACLD) patch treatments. Sampath, Balachandran (1999) presented analytical and experimental investigations on active (LMS feed-forward) control of multiple tones transmitted into a three-dimensional rectangular panel-enclosure system by using multiple piezoelectric actuators. Kim *et al.* (1999) utilized finite element modeling to study the response of a piezoelectric smart structure consisting of an aluminum plate with a surface-mounted circular piezoelectric actuator/sensor pair for active noise reduction within a cubic-shaped cavity. Azzouz, Ro (2002) developed a finite element model to numerically simulate an ACLD (Active Constrained Layer Damping) treated rectangular plate/acoustic cavity system excited by a point harmonic force over broad frequency bands. Ray, Reddy (2004) developed a finite element model to investigate active structural acoustic control (ASAC) of a thin laminated composite plate coupled to a rectangular parallelepiped acoustic cavity by using active constrained layer damping (ACLD) treatment. Al-Bassyiouni, Balachandran (2005) developed a zero-spillover feed-forward controller for attenuation of both narrowband and broadband three-dimensional sound fields within a rectangular enclosure with a flexible boundary containing surface-bonded piezo-actuator patches. Ray *et al.* (2009) developed a coupled structural-acoustic finite element model for controlling sound radiation from a vibrating thin laminated composite plate integrated with vertically reinforced 1–3 PFRC material into a backing rectangular parallelepiped acoustic cavity. Casadei *et al.* (2010) presented a coupled finite element model to evaluate noise reduction performance of a flexible rectangular plate containing a periodic array of tunable resistive-inductive (RL) shunted piezoelectric patches within an enclosed rectangular cavity. Jin *et al.* (2011) offered an analytical study on active control of sound transmission into a cabin-like enclosure comprising of two parallel flexible plates using three different control system configurations.

The presented state of art clearly shows that the use of various control methods to attenuate sound transmission through (radiation from) flexible enclosure boundaries of rectangular geometry has been under continual focus of the scientific community. In contrast, there appears to be no rigorous theoretical studies on the transient vibroacoustic response control of a circular plate structure coupled to a backing cylindrical enclosure (see Fig. 1). Thus, in this work, we shall take advantage of the linear acoustic wave equation, classical Rayleigh integral formula (Junger, Feit, 1986), Kirchhoff piezo-coupled plate model (Wang *et al.*, 2001), and Durbin's numerical Laplace transform inversion scheme (Durbin, 1973) in conjunction with the active damping control (ADC) strategy (Hasheminejad, Rabbani, 2015), to fill this important gap in the literature. The proposed model, which takes full account of interaction between vibrating panel and internal cavity fluid, is of both academic and industrial interest as a canonical problem in structural acoustics. The presented set of converged space-time solutions can provide further physical insights into the transient sound radiation characteristics of smart cylindrical cavity-coupled structural systems with a wide range of potential engineering applications (e.g., cavity resonators (Yang *et al.*, 2007), endplates and internal bulkheads in submarine hulls (Caresta, Kessissoglou, 2010), launch vehicles (Niezrecki, Cudney, 2001), and sounding rockets (Comrie, Korde, 2012). It can also serve as the benchmark data for confirmation of other solutions obtained by asymptotic or strictly numerical procedures (Cheng, Nicolas, 1992; Ro, Baz, 1999; Kim *et al.*, 1999; Ray, Reddy, 2004).
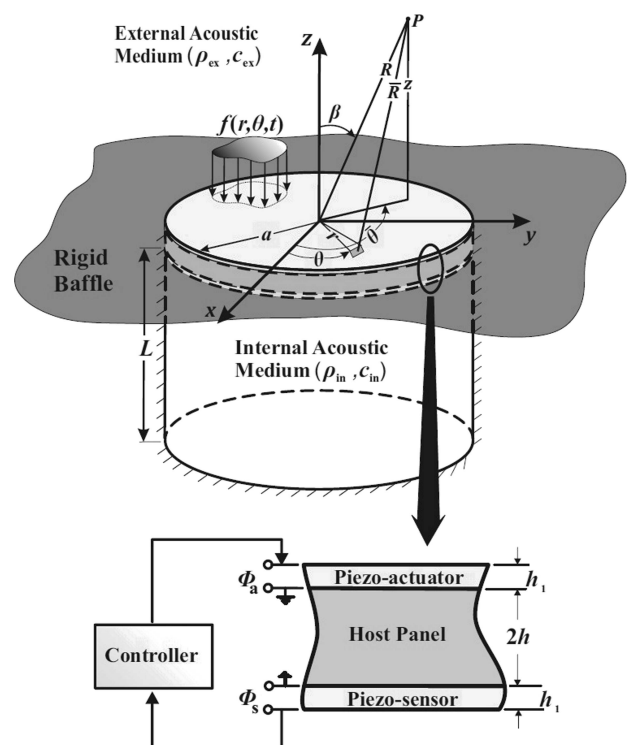
Fig. 1. Problem configuration.

2. Formulation

The basic problem configuration is illustrated in Fig. 1. The tri-laminate piezo-coupled circular plate $(0 \leq r \leq a)$ is comprised of an elastic isotropic host layer of thickness $2h$ that is perfectly joined to the top and bottom piezoelectric actuator and sensor layers of equal thickness h_1. It is assumed to be set in an infinite rigid baffle while subjected to an arbitrary transient external excitation $f(r, \theta, t)$ on its top surface. Furthermore, it is supposed to be clamped at its outer edge $(r = a)$, and coupled with a backing rigid-walled cylindrical acoustic enclosure $(\rho_{\text{in}}, c_{\text{in}})$ of finite depth L, with ρ_{in} denoting the cavity fluid density and c_{in} being the associated speed of sound. The composite panel radiates sound into the upper semi-infinite acoustic medium of the characteristic impedance, $\rho_{\text{ex}} c_{\text{ex}}$, with ρ_{ex} referring to the external fluid density (air in this case) and c_{ex} being the associated sound speed. Here, it should be noted that, as the overlaying acoustic half-space medium is assumed to be a light fluid (air) in the present study, its associated fluid loading effect on the vibrating panel is entirely neglected (JUNGER, FEIT, 1986), while that of the internal cavity fluid will be fully taken into account (HASHEMINEJAD et al., 2012). In what follows, in order to avoid unnecessary lengthy duplications, we shall briefly present the basic mathematical model of our coupled multi-field problem by making extensive use of the relevant results provided in selected references (HASHEMINEJAD, RABBANI, 2015; WANG et al., 2001; HASHEMINEJAD et al., 2012; GORMAN et al., 2001). In particular, the essential acoustic relations are given in Subsec. 2.1 (HASHEMINEJAD et al., 2012; GORMAN et al., 2001), the basic structural model is briefly introduced in Subsec. 2.2 (WANG et al., 2001), the associated structure/fluid compatibility relation is implemented in Subsec. 2.3 (HASHEMINEJAD et al., 2012; GORMAN et al., 2001), the active damping control (ADC) strategy is shortly described in Subsec. 2.4 (HASHEMINEJAD, RABBANI, 2015), and the final governing equations are derived in Subsec. 2.5.

2.1. Acoustic model

Adopting a time-domain approach based on the general 3D (non-axisymmetric) linear acoustic model, the perturbed acoustic velocity potential within the acoustic cavity, $\phi(r, \theta, z, t)$ is governed by the classic wave equation in cylindrical coordinates (GORMAN et al., 2001):

$$\nabla^2 \phi = \frac{1}{c_{\text{in}}^2} \frac{\partial^2 \phi}{\partial t^2}, \quad (1)$$

where t is time, and $\nabla^2 = \frac{\partial^2}{\partial r^2} + \frac{1}{r}\frac{\partial}{\partial r} + \frac{1}{r^2}\frac{\partial^2}{\partial \theta^2} + \frac{\partial^2}{\partial z^2}$. With direct application of Laplace transform with respect to time $\left(\overline{\Lambda}(r, \theta, z, s) = \int\limits_0^\infty \Lambda(r, \theta, z, t)e^{-st}\,\mathrm{d}t\right.$

with s being the transform parameter; assuming zero initial conditions), the wave Eq. (1) transforms into

$$\frac{\partial^2 \overline{\phi}}{\partial r^2} + \frac{1}{r}\frac{\partial \overline{\phi}}{\partial r} + \frac{1}{r^2}\frac{\partial^2 \overline{\phi}}{\partial \theta^2} + \frac{\partial^2 \overline{\phi}}{\partial z^2} - \left(\frac{s}{c_{\text{in}}}\right)^2 \overline{\phi} = 0, \quad (2)$$

where "over-bar" hereafter denotes the Laplace transform with respect to time. Also, following the standard method of separation of variables, after application of the enclosure rigid-surface conditions (HASHEMINEJAD et al., 2012; GORMAN et al., 2001):

$$\left.\frac{\partial \overline{\phi}}{\partial z}\right|_{z=-L} = \left.\frac{\partial \overline{\phi}}{\partial r}\right|_{r=a} = 0, \quad (3)$$

the solution to Eq. (2) is expressed in the form

$$\overline{\phi}(r, \theta, z, s) = \sum_{n=0}^\infty \sum_{m=0}^\infty A_{nm}(s)\Omega_{nm}(r, \theta)[\cos(\gamma_{nm} z)$$
$$- \tan(\gamma_{nm} L)\sin(\gamma_{nm} z)], \quad (4)$$

where $\Omega_{nm}(r, \theta) = J_m(\lambda_{nm} r)\cos m\theta$, J_m is the cylindrical Bessel function of first kind (ABRAMOWITZ, STEGUN, 1964), $\gamma_{nm}^2 = -\lambda_{nm}^2 - \left(\frac{s}{c_{\text{in}}}\right)^2$, in which λ_{nm} $(n, m = 0, 1, 2, 3, \ldots)$ are roots of the characteristic equation $J_m'(\lambda a) = 0$, and $A_{nm}(s)$ are the unknown modal constants.

2.2. Structural model

In this subsection, we shall adopt the formulation results presented in (WANG et al., 2001) where the free vibration analysis of piezoelectric coupled circular plate is based on Kirchhoff's classical (thin) plate theory (i.e., the shear deformation and rotary inertia effects are neglected). Furthermore, a quadratic electrical distribution in thickness direction of the closed circuit piezoelectric layer is assumed such that the Maxwell static electricity equation is satisfied. Here, for the sake of brevity, we shall only present the essential governing equations of the piezo-coupled sandwich panel, and the interested reader is referred to (WANG et al., 2001) for more details on the subject. Accordingly, assuming that the piezo-coupled plate undergoes small vibratory motion, the panel displacement field may be described by the classical relations (WANG et al., 2001),

$$u_z(r, \theta, t) = w(r, \theta, t),$$
$$u_r(r, \theta, t) = -z\frac{\partial w}{\partial r}, \quad (5)$$
$$u_\theta(r, \theta, t) = -z\frac{\partial w}{r\partial \theta},$$

where $u_z = w$, u_r and u_θ refer to the displacement components in the transverse, radial, and tangential

directions, respectively. Also, the relevant stress components in the host isotropic layer are readily obtained from (WANG et al., 2001)

$$
\sigma_{rr} = \frac{E}{1-\nu^2} \left[\frac{\partial u_r}{\partial r} + \nu \left(\frac{\partial u_\theta}{r \partial \theta} + \frac{u_r}{r} \right) \right]
$$
$$
= -\frac{zE}{1-\nu^2} \left[\frac{\partial^2 w}{\partial r^2} + \nu \left(\frac{1}{r}\frac{\partial w}{\partial r} + \frac{1}{r^2}\frac{\partial^2 w}{\partial \theta^2} \right) \right],
$$

$$
\sigma_{\theta\theta} = \frac{E}{1-\nu^2} \left[\left(\frac{\partial u_\theta}{r \partial \theta} + \frac{u_r}{r} \right) + \nu \frac{\partial u_r}{\partial r} \right]
$$
$$
= -\frac{zE}{1-\nu^2} \left[\frac{1}{r}\frac{\partial w}{\partial r} + \frac{1}{r^2}\frac{\partial^2 w}{\partial \theta^2} + \nu \frac{\partial^2 w}{\partial r^2} \right], \quad (6)
$$

$$
\sigma_{r\theta} = \frac{G}{2} \left(\frac{1}{r}\frac{\partial u_r}{\partial \theta} + \frac{\partial u_\theta}{\partial r} - \frac{u_\theta}{r} \right)
$$
$$
= -\frac{zE}{1+\nu} \left(\frac{1}{r}\frac{\partial^2 w}{\partial r \partial \theta} - \frac{1}{r^2}\frac{\partial w}{\partial \theta} \right),
$$

with E and ν being the Young's modulus and Poisson's ratio, respectively. Similarly, the stress components in the piezoelectric material are written as (WANG et al., 2001)

$$
\Sigma_{rr} = C_{11}\frac{\partial u_r}{\partial r} + C_{12}\left(\frac{\partial u_\theta}{r \partial \theta} + \frac{u_r}{r} \right) - e_{31}E_z,
$$
$$
\Sigma_{\theta\theta} = C_{12}\frac{\partial u_r}{\partial r} + C_{11}\left(\frac{\partial u_\theta}{r \partial \theta} + \frac{u_r}{r} \right) - e_{31}E_z, \quad (7)
$$
$$
\Sigma_{r\theta} = (C_{11} - C_{12})\frac{1}{2}\left(\frac{1}{r}\frac{\partial u_r}{\partial \theta} + \frac{\partial u_\theta}{\partial r} - \frac{u_\theta}{r} \right),
$$

where C_{11}, C_{12} and e_{31} are the material constants, as defined in Appendix, and the relevant electric field components, (E_r, E_θ, E_z), are defined (in terms of electric potential) in Eqs. (30) of Appendix.

Now, assuming that the piezoelectric layers are poled in the thickness (z-) direction, the total electric potential can be written as the superposition of the electric potential distributions induced on the top/bottom electrode surfaces of the actuator/sensor (Φ_a, Φ_s) layers (WANG et al., 2001):

$$
\Phi(r,\theta,z,t) = \frac{1}{h_1^3}(z+h+h_1)(z^2-h^2)\Phi_a(r,\theta,t)
$$
$$
+ \frac{1}{h_1^3}(z-h-h_1)(z^2-h^2)\Phi_s(r,\theta,t). \quad (8)
$$

Accordingly, the resultant shear force components (q_r, q_θ), based on the resultant moment $(M_{rr}, M_{\theta\theta}, M_{r\theta})$ expressions provided in Eqs. (32) of Appendix, are written in the form (WANG et al., 2001)

$$
q_r = \frac{\partial M_{rr}}{\partial r} + \frac{1}{r}\frac{\partial M_{r\theta}}{\partial \theta} + \frac{M_{rr} - M_{\theta\theta}}{r}
$$
$$
= -\left[(D_1 + D_2)\frac{\partial}{\partial r}\left(\nabla^2 w \right) \right.
$$
$$
\left. - D_3 e_{31}\frac{\partial \Phi_s}{\partial r} - D_4 e_{31}\frac{\partial \Phi_a}{\partial r} \right],
$$
$$
\quad (9)
$$
$$
q_\theta = \frac{\partial M_{r\theta}}{\partial r} + \frac{1}{r}\frac{\partial M_{\theta\theta}}{\partial \theta} + \frac{2M_{r\theta}}{r}
$$
$$
= -\frac{1}{r}\left[(D_1 + D_2)\frac{\partial}{\partial \theta}\left(\nabla^2 w \right) \right.
$$
$$
\left. - D_3 e_{31}\frac{\partial \Phi_s}{\partial \theta} - D_4 e_{31}\frac{\partial \Phi_a}{\partial \theta} \right],
$$

where $\nabla^2 = \frac{\partial^2}{\partial r^2} + \frac{1}{r}\frac{\partial}{\partial r} + \frac{1}{r^2}\frac{\partial^2}{\partial \theta^2}$, and

$$
D_1 = \frac{2Eh^3}{3(1-\nu^2)},
$$
$$
D_2 = \frac{2}{3}h_1\left(3h^2 + 3hh_1 + h_1^2 \right)C_{11},
$$
$$
D_3 = \left(\frac{2}{3}h + \frac{1}{6}h_1 \right),
$$
$$
D_4 = \frac{1}{6h_1^2}\left(48h^3 + 96h^2 h_1 + 68hh_1^2 + 17h_1^3 \right).
$$

Direct substitution of the shear force expressions (9) into the following classic governing equation of motion for the Kirchhoff plate (RAO, 2007):

$$
\frac{\partial q_r}{\partial r} + \frac{1}{r}\frac{\partial q_\theta}{\partial \theta} + \frac{q_r}{r} + F
$$
$$
- \left[\int_{-h}^{h} \rho_h \frac{\partial^2 w}{\partial t^2}dz + 2\int_{h}^{h+h_1} \rho_p \frac{\partial^2 w}{\partial t^2}\,\mathrm{d}z \right] = 0, \quad (10)
$$

results into,

$$
(D_1 + D_2)\nabla^4 w - e_{31}D_3\nabla^2 \Phi_s - e_{31}D_4\nabla^2 \Phi_a
$$
$$
+ 2(\rho_h h + \rho_p h_1)\frac{\partial^2 w}{\partial t^2} = F, \quad (11)
$$

where ρ_h and ρ_p are material densities of the host plate and piezoelectric layers, respectively, $F(r,\theta,t) = p_{in}(r,\theta,z=0,t) - f(r,\theta,t)$ is the generalized applied force (where we have adopted the light external fluid hypothesis (JUNGER, FEIT, 1986)), and p_{in} denotes the acoustic pressure within the cylindrical enclosure, which by making use of expansion (4) can be written in the Laplace domain as (HASHEMINEJAD et al., 2012)

$$
\overline{p}_{in}(r,\theta,z,s) = -\rho_{in}s\overline{\phi}
$$
$$
= -\rho_{in}s\sum_{n=0}^{\infty}\sum_{m=0}^{\infty} A_{nm}(s)\Omega_{nm}(r,\theta) \quad (12)
$$
$$
\cdot [\cos(\gamma_{nm}z) - \tan(\gamma_{nm}L)\sin(\gamma_{nm}z)].
$$

Direct substitution of Eqs. (31) (of Appendix) for the relevant electric displacement components, (D_r, D_θ, D_z), into the following classical Maxwell equation (DUAN *et al.*, 2005):

$$\int\limits_h^{h+h_1} \left[\frac{1}{r}D_r + \frac{\partial D_r}{\partial r} + \frac{1}{r}\frac{\partial D_\theta}{\partial \theta} + \frac{\partial D_z}{\partial z} \right] dz = 0, \quad (13)$$

after some manipulations leads to

$$\Xi_{11}\frac{D_3}{2}\nabla^2\Phi_s - \Xi_{33}D_6\Phi_s - \Xi_{11}D_5\nabla^2\Phi_a$$
$$- \Xi_{33}D_7\Phi_a - e_{31}h_1\nabla^2 w = 0, \quad (14)$$

where Ξ_{11} and Ξ_{33} are reduced dielectric constants of the piezoelectric layers (see Appendix), and $D_5 = \frac{1}{12h_1}\left(24h^2 + 28hh_1 + 7h_1^2\right)$, $D_6 = (4h + h_1)/h_1^2$, $D_7 = (8h + 5h_1)/h_1^2$. Elimination of $\nabla^2\Phi_s$ between Eqs. (11) and (14) leads to the expression for the sensor voltage in the form

$$\Phi_s(r,\theta,t) = B_1\nabla^4 w - B_2\nabla^2\Phi_a$$
$$- B_3\Phi_a - B_4\nabla^2 w + B_5\ddot{w} + B_6 F, \quad (15)$$

where

$$B_1 = \frac{\Xi_{11}(D_1 + D_2)}{2\Xi_{33}e_{31}D_6}, \qquad B_2 = \frac{\Xi_{11}(2D_5 + D_4)}{2\Xi_{33}D_6},$$

$$B_3 = \frac{D_7}{D_6}, \qquad B_4 = \frac{e_{31}h_1}{\Xi_{33}D_6},$$

$$B_5 = \frac{\Xi_{11}(\rho_h h + \rho_p h_1)}{e_{31}\Xi_{33}D_6}, \qquad B_6 = \frac{\Xi_{11}}{2\Xi_{33}e_{31}D_6}.$$

Applying the Laplace operator to Eq. (15), and direct substitution of results into Eq. (11), after taking the Laplace transform with respect to time (assuming zero initial conditions), yields the final equation of motion for forced vibrations of the piezo-coupled circular plate in the form

$$P_3\nabla^6\overline{w} - P_2\nabla^4\overline{w} + s^2 P_1\nabla^2\overline{w} - s^2 P_0\overline{w}$$
$$= \overline{F} - P_4\nabla^2\overline{F} + P_5\nabla^2\overline{\Phi}_a + P_6\nabla^4\overline{\Phi}_a, \quad (16)$$

where

$$P_0 = 2(\rho_h h + \rho_p h_1),$$

$$P_1 = \frac{\Xi_{11}D_3}{\Xi_{33}D_6}(\rho_h h + \rho_p h_1),$$

$$P_2 = \left(D_1 + D_2 + \frac{e_{31}^2 h_1 D_3}{\Xi_{33}D_6} \right),$$

$$P_3 = \frac{\Xi_{11}D_3}{2\Xi_{33}D_6}(D_1 + D_2),$$

$$P_4 = \frac{\Xi_{11}D_3}{2\Xi_{33}D_6},$$

$$P_5 = \frac{e_{31}D_3 D_7}{D_6} - e_{31}D_4,$$

$$P_6 = \frac{e_{31}\Xi_{11}D_3}{2\Xi_{33}D_6}(2D_5 + D_4),$$

with the general solution

$$\overline{w}(r,\theta,s) = \sum_{n=0}^{\infty}\sum_{m=0}^{\infty} Q_{nm}(s)W_{nm}(r,\theta), \quad (17)$$

where $Q_{nm}(s)(n,m = 0,1,2,\ldots)$ are unknown constants, and $W_{nm}(r,\theta)$ refer to the free vibrational mode shapes of the (dry) piezo-coupled circular plate with the general form (WANG *et al.*, 2001):

$$W_{nm}(r,\theta) = \Big[M_{1nm}\Pi_{1nm}(\sqrt{|x_1|}r)$$
$$+ M_{2nm}\Pi_{2nm}(\sqrt{|x_2|}r)$$
$$+ M_{3nm}\Pi_{3nm}(\sqrt{|x_3|}r) \Big]\cos m\theta, \quad (18)$$

where

$$\Pi_{inm}\left(\sqrt{|x_i|}r\right) = \begin{cases} J_m(\sqrt{|x_i|}r), & x_i < 0 \\ I_m(\sqrt{|x_i|}r), & x_i > 0 \end{cases} \quad (i = 1,2,3)$$

in which I_m is the modified cylindrical Bessel function of the first kind, $M_{inm}(i = 1,2,3)$ are mode shape constants, the parameters $x_{1,2,3}$ (which are related to the system natural frequencies ω_{nm}) are roots of the associated characteristic equation, as given in Eq. (54) of (WANG *et al.*, 2001).

2.3. Fluid/structure compatibility

Next, we are ready to impose the last remaining boundary condition. In particular, the continuity of internal fluid particle velocity with the piezo-elastic plate velocity at $z = 0$ implies that (HASHEMINEJAD *et al.*, 2012; GORMAN *et al.*, 2001)

$$\left.\frac{\partial\overline{\phi}}{\partial z}\right|_{z=0} = s\overline{w}(r,\theta,s). \quad (19)$$

By direct substitution of expansions (4) and (17) into the above fluid/structure compatibility relation, one obtains

$$-\sum_{n=0}^{\infty}\sum_{m=0}^{\infty} A_{nm}(s)\gamma_{nm}\Omega_{nm}(r,\theta)\tan(\gamma_{nm}L)$$
$$= \sum_{n=0}^{\infty}\sum_{m=0}^{\infty} Q_{nm}(s)W_{nm}(r,\theta). \quad (20)$$

Multiplying the above equation by $W_{ij}(r,\theta)$ and integrating over the circular panel surface area one obtains

$$\sum_{n=0}^{\infty}\sum_{m=0}^{\infty} A_{nm}(s)H_{nmij} = \sum_{n=0}^{\infty}\sum_{m=0}^{\infty} Q_{nm}(s)K_{nmij}, \quad (21)$$

where

$$H_{nmij} = -\gamma_{nm} \tan(\gamma_{nm}L) \iint\limits_{A} \Omega_{nm}(r,\theta)W_{ij}(r,\theta)\, \mathrm{d}A,$$

$$K_{nmij} = s \iint\limits_{A} W_{nm}(r,\theta)W_{ij}(r,\theta)\, \mathrm{d}A,$$

in which $i,j,n,m = 0,1,2,\ldots$, and $\mathrm{d}A = r\,\mathrm{d}r\,\mathrm{d}\theta$.

2.4. Controller design

Now, following the controller design procedure presented in (HASHEMINEJAD, RABBANI, 2015; VEL, BAILLARGEON, 2005), we shall apply the active damping control (ADC) strategy as a proportional voltage feedback controller to our cavity-coupled smart panel system (see Fig. 1). This can be readily achieved through a second order compensator forced by the sensor electric potential (Φ_{s}) measured at an arbitrary point ($r = r_0$, $\theta = \theta_0$, $z = -h - h_1$) on the lower surface of the piezo-composite panel (HASHEMINEJAD, RABBANI, 2015), i.e,

$$\ddot{\eta}_{\mathrm{a}} + 2\xi_c\omega_c\dot{\eta}_{\mathrm{a}} + \omega_c^2\eta_{\mathrm{a}} = k_{\mathrm{p}}\omega_c^2\alpha\Phi_{\mathrm{s}}(r_0,\theta_0,t), \qquad (22)$$

where k_{p} is the controller gain,

$$\alpha = -2(h + h_1)(2h + h_1)/h_1^2,$$

$\eta_{\mathrm{a}}(t)$ is the controller coordinate, and ω_c and ξ_c refer to the natural frequency and damping ratio of the controller, respectively. Taking Laplace transform of the above equation, and solving for the controller coordinate, one gets

$$\overline{\eta}_{\mathrm{a}}(s) = T(s)\overline{\Phi}_{\mathrm{s}}(r_0,\theta_0,s), \qquad (23)$$

where $T(s) = k_{\mathrm{p}}\omega_c^2\alpha/\left(s^2 + 2\xi_c\omega_c s + \omega_c^2\right)$ is the controller transfer function, and the transformed sensor voltage can readily be obtained from Eq. (15).

2.5. Final governing equations

At this point, by decomposition of the actuator voltage in the form $\overline{\Phi}_{\mathrm{a}}(r,\theta,s) = \overline{\eta}_{\mathrm{a}}(s)\varphi_{\mathrm{a}}(r,\theta)$, and direct substitution of Eq. (17) into the equation of motion (16), while noting that the normal modes, $W_{nm}(r,\theta)$ must satisfy the free vibration eigen-relation $P_3\nabla^6 W_{nm} - P_2\nabla^4 W_{nm} = \omega_{nm}^2\left(P_1\nabla^2 W_{nm} - P_0 W_{nm}\right)$ one obtains

$$\sum_{n=0}^{\infty}\sum_{m=0}^{\infty} Q_{nm}(s)(\omega_{nm}^2 + s^2)(P_1\nabla^2 W_{nm} - P_0 W_{nm})$$

$$= -s\rho_{\mathrm{in}}\sum_{n=0}^{\infty}\sum_{m=0}^{\infty} A_{nm}(s)\Omega_{nm}(r,\theta) - \overline{f}(r,\theta,s)$$

$$+ s\rho_{\mathrm{in}}P_4\sum_{n=0}^{\infty}\sum_{m=0}^{\infty} A_{nm}(s)\nabla^2\Omega_{nm}(r,\theta)$$

$$+ P_4\nabla^2\overline{f}(r,\theta,s) + \overline{\eta}_{\mathrm{a}}(s)\left(P_5\nabla^2\varphi_{\mathrm{a}} + P_6\nabla^4\varphi_{\mathrm{a}}\right). \quad (24)$$

Also, direct implementation of pressure and displacement field expansions (12) and (17) into the controller coordinate Eq. (23), keeping Eq. (15) in mind, yields

$$\left[\frac{1}{T(s)} + \left(B_2\nabla^2\varphi_{\mathrm{a}}(r_0,\theta_0) + B_3\varphi_{\mathrm{a}}(r_0,\theta_0)\right)\right]\overline{\eta}_{\mathrm{a}}(s)$$

$$= \sum_{n=0}^{\infty}\sum_{m=0}^{\infty} Q_{nm}(s)\Psi_{nm}(r_0,\theta_0,s) - B_6\overline{f}(r_0,\theta_0,s)$$

$$- s\rho_{\mathrm{in}}B_6\sum_{n=0}^{\infty}\sum_{m=0}^{\infty} A_{nm}(s)\Omega_{nm}(r_0,\theta_0), \qquad (25)$$

where

$$\Psi_{nm}(r_0,\theta_0,s) = B_1\nabla^4 W_{nm}(r_0,\theta_0)$$

$$- B_4\nabla^2 W_{nm}(r_0,\theta_0)$$

$$+ s^2 B_5 W_{nm}(r_0,\theta_0).$$

Finally, multiplication of Eqs. (24) and (25) through by $W_{ij}(r,\theta)$, and subsequent integration on circular surface area of the panel respectively leads to

$$\sum_{n=0}^{\infty}\sum_{m=0}^{\infty} Q_{nm}(s)Z_{nmij} = S_{ij}^{(1)} + \overline{\eta}_{\mathrm{a}}(s)S_{ij}^{(2)}$$

$$+ \sum_{n=0}^{\infty}\sum_{m=0}^{\infty} A_{nm}(s)X_{nmij},$$

$$S_{ij}^{(3)}\overline{\eta}_{\mathrm{a}}(s) = \sum_{n=0}^{\infty}\sum_{m=0}^{\infty} Q_{nm}(s)\Upsilon_{nmij} - S_{ij}^{(4)}$$

$$- \sum_{n=0}^{\infty}\sum_{m=0}^{\infty} A_{nm}(s)\Gamma_{nmij}, \qquad (26)$$

where

$$Z_{nmij} = (\omega_{nm}^2 + s^2)\iint\limits_{A} W_{ij}\left[P_1\nabla^2 W_{nm} - P_0 W_{nm}\right]\mathrm{d}A,$$

$$X_{nmij} = s\rho_{\mathrm{in}}\iint\limits_{A} W_{ij}\left[P_4\nabla^2\Omega_{nm} - \Omega_{nm}\right]\mathrm{d}A,$$

$$\Upsilon_{nmij} = \Psi_{nm}(r_0,\theta_0,s)\iint\limits_{A} W_{ij}\,\mathrm{d}A,$$

$$\Gamma_{nmij} = \rho_{\mathrm{in}}sB_6\Omega_{nm}(r_0,\theta_0)\iint\limits_{A} W_{ij}\,\mathrm{d}A,$$

$$S_{ij}^{(1)} = \iint\limits_{A} W_{ij}\left[P_4\nabla^2\overline{f} - \overline{f}\right]\mathrm{d}A,$$

$$S_{ij}^{(2)} = \iint\limits_{A} W_{ij}\left(P_5\nabla^2\varphi_{\mathrm{a}} + P_6\nabla^4\varphi_{\mathrm{a}}\right)\mathrm{d}A,$$

$$S_{ij}^{(3)} = \left[\frac{1}{T(s)} + \left(B_2 \nabla^2 \varphi_{\mathrm{a}}(r_0, \theta_0) + B_3 \varphi_{\mathrm{a}}(r_0, \theta_0) \right) \right]$$
$$\cdot \iint\limits_A W_{ij} \, \mathrm{d}A,$$

$$S_{ij}^{(4)} = B_6 \overline{f}(r_0, \theta_0, s) \iint\limits_A W_{ij} \, \mathrm{d}A,$$

Thus, by truncating the linear systems of Eqs. (21) and (26), with M being the truncation constant, one advantageously arrives at the final set of matrix equations:

$$\mathbf{H}(s)\mathbf{A}(s) = \mathbf{K}(s)\mathbf{Q}(s),$$

$$\mathbf{Z}(s)\mathbf{Q}(s) = \mathbf{S}_1(s) + \mathbf{S}_2(s)\overline{\eta}_{\mathrm{a}}(s) + \mathbf{X}(s)\mathbf{A}(s), \quad (27)$$

$$\mathbf{S}_3(s)\overline{\eta}_{\mathrm{a}}(s) = \boldsymbol{\Upsilon}(s)\mathbf{Q}(s) - \mathbf{S}_4(s) - \boldsymbol{\Gamma}(s)\mathbf{A}(s),$$

where

$$\mathbf{Q}(s) = [Q_{00}(s), Q_{01}(s), \ldots,$$
$$Q_{0M}(s), Q_{10}(s), Q_{11}(s), \ldots, Q_{1M}(s), \ldots,$$
$$Q_{M0}(s), Q_{M1}(s), \ldots, Q_{MM}(s)]^{\mathrm{T}},$$

$$\mathbf{A}(s) = [A_{00}(s), A_{01}(s), \ldots,$$
$$A_{0M}(s), A_{10}(s), A_{11}(s), \ldots,$$
$$A_{1M}(s), \ldots, A_{M0}(s), A_{M1}(s), \ldots, A_{MM}(s)]^{\mathrm{T}},$$

$$\mathbf{S}_i(s) = [S_{00}^{(i)}(s), S_{01}^{(i)}(s), \ldots,$$
$$S_{0M}^{(i)}(s), S_{10}^{(i)}(s), S_{11}^{(i)}(s), \ldots,$$
$$S_{1M}^{(i)}(s), \ldots, S_{M0}^{(i)}(s), S_{M1}^{(i)}(s), \ldots, S_{MM}^{(i)}(s)]^{\mathrm{T}},$$

in which $i = 1, 2, 3, 4$, and the coefficient matrices in Eq. (27) are of general form:

$$\boldsymbol{\mathcal{H}}(s) = \begin{bmatrix} \mathcal{H}_{0000} & \ldots & \mathcal{H}_{0M00} & & \mathcal{H}_{M000} & \ldots & \mathcal{H}_{MM00} \\ \vdots & \ddots & \vdots & \cdots & \vdots & \ddots & \vdots \\ \mathcal{H}_{000M} & \ldots & \mathcal{H}_{0M0M} & & \mathcal{H}_{M00M} & \ldots & \mathcal{H}_{MM0M} \\ \vdots & & \vdots & \ddots & & \vdots & \\ \mathcal{H}_{00M0} & \ldots & \mathcal{H}_{0MM0} & & \mathcal{H}_{M0M0} & \ldots & \mathcal{H}_{MMM0} \\ \vdots & \ddots & \vdots & \cdots & \vdots & \ddots & \vdots \\ \mathcal{H}_{00MM} & \ldots & \mathcal{H}_{0MMM} & & \mathcal{H}_{M0MM} & \ldots & \mathcal{H}_{MMMM} \end{bmatrix}$$

where $\boldsymbol{\mathcal{H}}(s) = [\mathcal{H}_{nmij}]$ can be any of $\mathbf{H}(s) = [H_{nmij}]$, $\mathbf{K}(s) = [K_{nmij}]$, $\mathbf{Z}(s) = [Z_{nmij}]$, $\mathbf{X}(s) = [X_{nmij}]$, $\boldsymbol{\Upsilon}(s) = [\Upsilon_{nmij}]$ and $\boldsymbol{\Gamma}(s) = [\Gamma_{nmij}]$. By simultaneous solution of the linear system of matrix Eqs. (27), one can ultimately determine the unknown coefficients $\mathbf{A}(s)$, $\mathbf{Q}(s)$ and $\overline{\eta}_{\mathrm{a}}(s)$ in the Laplace domain. This completes the mathematical modeling of the problem. Next, we consider some numerical examples.

3. Numerical results

Before presenting the main results of our numerical simulations, it should be mentioned here that the primary goal of proposed GA-tuned active damping control system is effective suppression of key acousto-structural parameters (i.e., panel displacement and radiated sound pressure amplitudes) with a reasonable control effort. Also, noticing the relatively large number of input parameters involved, while keeping in mind our computational hardware limitations, a specific model will be considered here. The external surrounding fluid is assumed to be air ($\rho_{\mathrm{ex}} = 1.2 \, \mathrm{kg/m^3}$, $c_{\mathrm{ex}} = 343 \, \mathrm{m/s}$), while the cavity fluid is taken to be either air or water ($\rho_{\mathrm{in}} = 1.2 \, \mathrm{kg/m^3}$, $1000 \, \mathrm{kg/m^3}$, $c_{\mathrm{in}} = 343 \, \mathrm{m/s}$, $1500 \, \mathrm{m/s}$), for selected cavity depth parameters ($L/2a = 0.1, 1, 10$). The core layer of the piezo-coupled circular plate ($a = 0.5 \, \mathrm{m}$) is supposed to be steel ($\nu = 0.3$, $\rho_h = 7800 \, \mathrm{kg/m^3}$, $E = 2.1 \times 10^{11} \, \mathrm{N/m^2}$, $2h = 0.01 \, \mathrm{m}$), with the physical properties of the thin PZT4 piezo-ceramic sensor/actuator layers ($h_1 = 0.001 \, \mathrm{m}$,), as given in Table 1. In all numerical simulations (except in validation), an impulsive central transverse point load is assumed to be acting on the top surface of the piezo-coupled panel ($r = \theta = 0$), which can be represented by $f(r, \theta, t) = F_0 \delta(r)\delta(\theta)\delta(t)$ with $F_0 = 4 \, \mathrm{kPa}$, where $\delta(.)$ is the Dirac delta function. Also, in the absence of material damping, ensuing the controller design procedure in (Vel, Baillargeon, 2005), the damping ratio of the controller is assumed to be $\xi_c = 0.1$, while the controller frequency is targeted at the fundamental frequency for free vibrations of the piezo-coupled clamped (dry) circular panel (Wang *et al.*, 2001) Furthermore, the input voltage Φ_{s} is measured at the point ($r = r_0 = 0.25 \, \mathrm{m}$, $\theta = \theta_0 = \pi/6$, $z = -0.006 \, \mathrm{m}$) on the lower surface of the sensor layer. Similarly, the actuation voltage, $\varphi_{\mathrm{a}}(r, \theta)$, is assumed to be imposed in an annular region ($0.2 \leq r \leq 0.3 \, \mathrm{m}$, $0 \leq \theta \leq 2\pi$, $z = +0.006 \, \mathrm{m}$) over the upper surface of the actuator layer. Moreover, the controller gain parameter, k_{p}, is tuned by utilizing the Genetic Algorithm (GA) capability of Matlab Global Optimiza-

Table 1. Physical properties of the constituent panel materials.

	Core steel layer	PZT4 layers
Elastic moduli [$\mathrm{N \cdot m^{-2}}$]	$E = 200 \cdot 10^9$	$\overline{c}_{11} = 132 \cdot 10^9$
		$\overline{c}_{12} = 71 \cdot 10^9$
		$\overline{c}_{33} = 115 \cdot 10^9$
		$\overline{c}_{13} = 73 \cdot 10^9$
Density [$\mathrm{kg \cdot m^{-3}}$]	$7.8 \cdot 10^3$	$7.5 \cdot 10^3$
$\overline{e}_{31}$ [$\mathrm{C \cdot m^{-2}}$]	–	-4.1
$\overline{e}_{33}$ [$\mathrm{C \cdot m^{-2}}$]	–	14.1
E_{11} [$\mathrm{F \cdot m^{-1}}$]	–	$7.124 \cdot 10^{-9}$
E_{33} [$\mathrm{F \cdot m^{-1}}$]	–	$5.841 \cdot 10^{-9}$

tion Toolbox in a multi-objective framework, where the principal objective functions, which account for evaluation of the solution at each step, are selected as the internal radiated (cavity center-point) sound pressure, $p_{\text{in}}(r = \theta = 0, z = -L/2, t)$ transverse panel center-point displacement, $w(r = \theta = 0, t)$ and the actuator input voltage, $\Phi_{\text{a}}(r = 0.25 \text{ m}, \theta = \pi/6, z = 0.006 \text{ m}, t)$, with maximum weight given to the panel displacement. For a detailed description of the GA-based controller gain optimization and weighting function selection procedure, the reader is referred to (HASHEMINEJAD, RABBANI, 2015).

With the hypothesis of light external fluid (air) loading, the radiated transient acoustic pressure field may be computed by making use of the following form of Rayleigh integral in Laplace domain (JUNGER, FEIT, 1986; SHAKERI, YOUNESIAN, 2015):

$$\overline{p}_{\text{ex}}\big(R, \beta, \overline{\theta}, s\big) = s^2 \frac{\rho_{\text{ex}}}{2\pi} \int\limits_{0}^{2\pi} \int\limits_{0}^{a} \frac{e^{i\overline{k}\,\overline{R}}}{\overline{R}} \overline{w}(r, \theta, s) r \, dr \, d\theta, \quad (28)$$

where

$$\overline{k} = is/c_{\text{ex}}, \qquad i = \sqrt{-1},$$

$$\overline{R} = \sqrt{R^2 + r^2 - 2rR\sin\beta\cos\big(\overline{\theta} - \theta\big)}$$

is the vector connecting a representative panel element $(dr, r \, d\theta)$ to the field point "P", as shown in Fig. 1, and the transformed panel displacement, $\overline{w}(r, \theta, s)$ is readily obtained from Eq. (17).

A general Maple code was constructed for simultaneous solution of the final truncated matrix Eqs. (27). In particular, in order to avoid further complications in the relatively complex problem formulation, and following the novel solution methodology described in (HASHEMINEJAD *et al.*, 2012; GORMAN *et al.*, 2001; 2008), the classical orthogonality properties of Bessel and transcendental functions (ABRAMOWITZ, STEGUN, 1964) need not to be applied in the current solution procedure. Alternatively, all integrations required in computation of elements of coefficient matrices that appear in the final set of Eqs. (27) (i.e., $\mathbf{H}(s)$, $\mathbf{K}(s)$, $\mathbf{Z}(s)$, $\mathbf{S}_{1-4}(s)$, $\mathbf{X}(s)$, $\mathbf{\Upsilon}(s)$, $\mathbf{\Gamma}(s)$), were performed numerically by making recurrent use of the adaptive Gaussian quadrature routine "Gquad" in Maple. Calculations were performed on a network of core i7-based desktop computers, and the convergence of numerical solutions was checked in a simple trial and error fashion, i.e., by accumulating the number of acousto-structural modes, while looking for steadiness in the numerical values of the outputs. Taking a maximum truncation constant of $M = 5$ was observed to lead to uniform convergence in all simulations. The inversion of Laplace transforms were numerically performed by making persistent use of the following Durbin's inversion formula in the interval $[0, 2T_0]$ (DURBIN, 1973; HASHEMINEJAD *et al.*, 2012):

$$\Lambda(t) = \frac{2e^{\mu t}}{T_0} \left[\frac{1}{2}\text{Re}\left[\overline{\Lambda}(\mu)\right] \right.$$

$$+ \sum_{k=1}^{\widehat{N}} \left\{ \text{Re}\left[\overline{\Lambda}\left(\mu + ik\frac{2\pi}{T_0}\right)\right]\cos\left(kt\frac{2\pi}{T_0}\right) \right.$$

$$\left. - \text{Im}\left[\overline{\Lambda}\left(\mu + ik\frac{2\pi}{T_0}\right)\right]\sin\left(kt\frac{2\pi}{T_0}\right)\right\}\right], \quad (29)$$

where $\widehat{N}$ is the truncation parameter, and μ is an arbitrary (real) number larger than all singularities of $\overline{\Lambda}(s)$, with the following selections: $\widehat{N} = 2000$, $\mu T_0 = 4.5$, $T_0 = 2$ s, for obtaining stable and convergent solutions.

Before getting to the main results, we shall briefly confirm the overall validity of the formulation. To do this we first computed the time histories of the transverse panel center-point displacement, $w(r = \theta = 0, t)$ the internal radiated (cavity center-point) sound pressure, $p_{\text{in}}(r = \theta = 0, z = -L/2, t)$ and the external radiated (on-axis) sound pressure, $p_{\text{ex}}(r = \theta = 0, z = 5a, t)$ due to a uniformly distributed step transverse load $(f(r, \theta, t) = F_0 = 4 \text{ kPa})$ acting over the cavity-coupled (air-filled; $L = 1$ m) piezo-laminated (PZT4-steel-PZT4) panel. Fair agreements are attained with the results calculated by using the commercial FEM package ABAQUS, as depicted in Fig. 2. About 3000
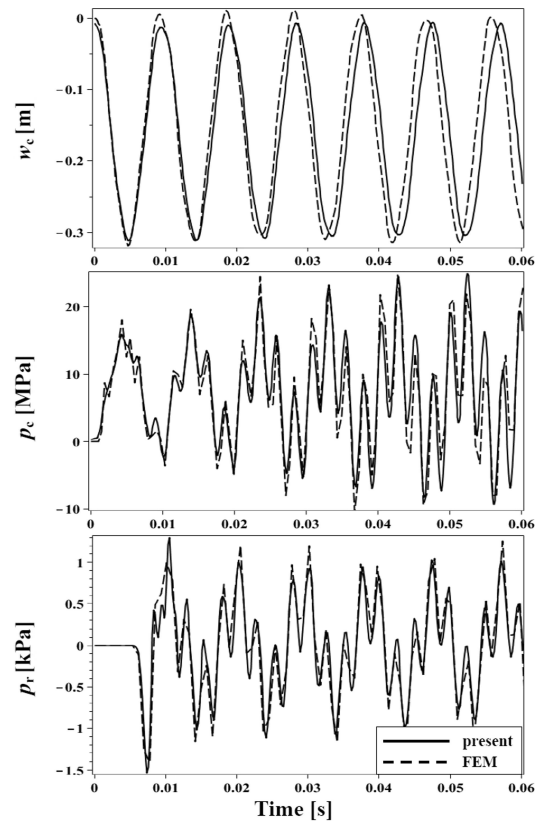
Fig. 2. Comparison of the calculated analytic solutions for a cavity-backed piezo-coupled circular panel with the FEM results.

C3D20RE (quadratic piezoelectric brick) elements were utilized to model the PZT4 sensor/actuator layers, and about 1300 C3D20R (quadratic brick) elements were employed to model the host steel layer in the ABAQUS model. Also, a total of about 200,000 AC3D20 (quadratic acoustic brick) elements were employed to model the external/internal acoustic mediums. As further checks for validity of the formulation, we used our basic (original) codes (in two different limiting situations) in order to calculate the first few natural frequencies for a piezo-coupled (PZT4-steel-PZT4) circular plate ($a = 0.6$ m, $2h = 0.02$ m, $h_1 = 0.002$ m) in the absence of fluid loading, as well as the resonance frequencies for an elastic isotropic (single-layer) cavity-backed (air-filled) circular (steel) panel ($a = 1$ m, $2h = 0.005$ m, $h_1 \approx 0$ m, $L = 6.72$ m). The outcome, as presented in Tables 2 and 3, show excellent agreements with those presented in (WANG *et al.*, 2001; GORMAN *et al.*, 2008), respectively.

Table 2. Comparison of the calculated natural frequencies of the piezo-coupled circular panel with those of Ref. (WANG *et al.*, 2001).

Mode	Present	Ref. (WANG *et al.*, 2001)
1	902.478	902.479
2	1878.169	1878.17
3	3081.079	3081.08
4	3513.432	3513.43

Table 3. Comparison of the calculated natural frequencies of the cavity-backed steel circular panel with those of Ref. (GORMAN *et al.*, 2008).

Mode	Present	Ref. (GORMAN *et al.*, 2008)
1	3.279	3.279
2	6.296	6.297
3	9.450	9.426

Figures 3a and 3b display the controlled and uncontrolled cavity center-point sound pressure, $p_c = p_{in}$ ($r = \theta = 0$, $z = -L/2$, t) (MPa) the on-axis external acoustic pressure, $p_r = p_{ex}$ ($R = 5a$, $\beta = \overline{\theta} = 0$, t) (kPa) transverse panel center-point displacement, $w_c = w(r = \theta = 0, t)$ (m) and the applied control voltage, Φ_a ($r = 0.25$ m, $\theta = \pi/6$, $z = 0.006$ m, t) (Volt), due to an impulsive central transverse point load ($f = 4\delta(r)\delta(\theta)\delta(t)$ kPa), for selected internal cavity fluids (air, water), and cavity depth parameters ($L/2a = 0.1$, 1, 10). The key observations are as follows. The panel displacement and acoustic pressure response curves associated with the water-filled cavity have a noticeably higher primary free oscillation frequency in comparison to those of the air-filled cavity. This is directly linked to the higher overall stiffness of the fully coupled water-filled sys-

tem in comparison to the air-filled system. Similarly, the stronger fluid-coupling effect of the water-filled cavity system leads to considerably lower panel displacements (w_c) and consequently radiated external pressure (p_r) amplitudes (see Eq. (28)) in comparison to the air-filled cavity system. Also, a substantial increase in the height of water-filled cavity (i.e., to $L/2a = 10$) leads to notable modification of the key acousto-structural parameters (w_c, p_c, p_r, Φ_a), which can directly be linked to the increased liquid (water) compressibility (wave field reverberation) effects (also note the short time delay observed in the associated p_c subplot). On the other hand, the depth of air-filled cavity is found to have no significant effect on the panel displacement and the resulting on-axis radiated external pressure (w_c, p_r), which can readily be connected to the well-known "light fluid loading" phenomenon (also note the relatively long time delay observed in the associated p_c subplot). Moreover, the efficiency of adopted control configuration in effective suppression of panel center-point displacement, w_c, as well as the resulting radiated on-axis (external) sound pressure, p_r, almost regardless of inner fluid type, especially for shorter cavities ($L/2a = 0.1$, 1), is evident in the figure. The internal acoustic pressure field, p_c on the other hand, behaves somewhat different. In particular, the control action becomes effective after about one full cycle of free panel oscillations with the highest attenuation levels observed for water-filled cavities of small to medium depths ($L/2a = 0.1$, 1) in moderate to late-times. This can evidently be linked to the increased level of control authority over internal pressure field for cavities of smaller depths, keeping in mind that maximum weight was allocated to the panel displacement in our multi-objective GA-based optimization scheme. The time variations of controlled panel displacement appear to roughly follow those of the associated applied control voltage (i.e., relatively high voltage levels are required in the early and moderate times, while lower actuator voltage levels are applied in late-times, especially for the water-filled cavity). Lastly, the effect of cavity depth on the control voltage is not very prominent, while the overall actuator voltage amplitude nearly doubles as the internal cavity fluid is changed from air to water. This is readily explained by the fact that an increased actuation power is naturally required for countering the higher fluid loading effects of the largely stiffer coupled water-filled cavity system.

The two-dimensional time-domain snapshots ($0.01 \leq t \leq 18$ ms) of Fig. 4 compare the controlled and uncontrolled internal radiated sound pressure fields, due to the impulsive central transverse point load ($f = 4\delta(r)\delta(\theta)\delta(t)$ kPa), for selected cavity depths ($L/2a = 0.1$, 1, 10), and internal fluid (water). Comments very similar to those made for Fig. 3 can

a)

b)
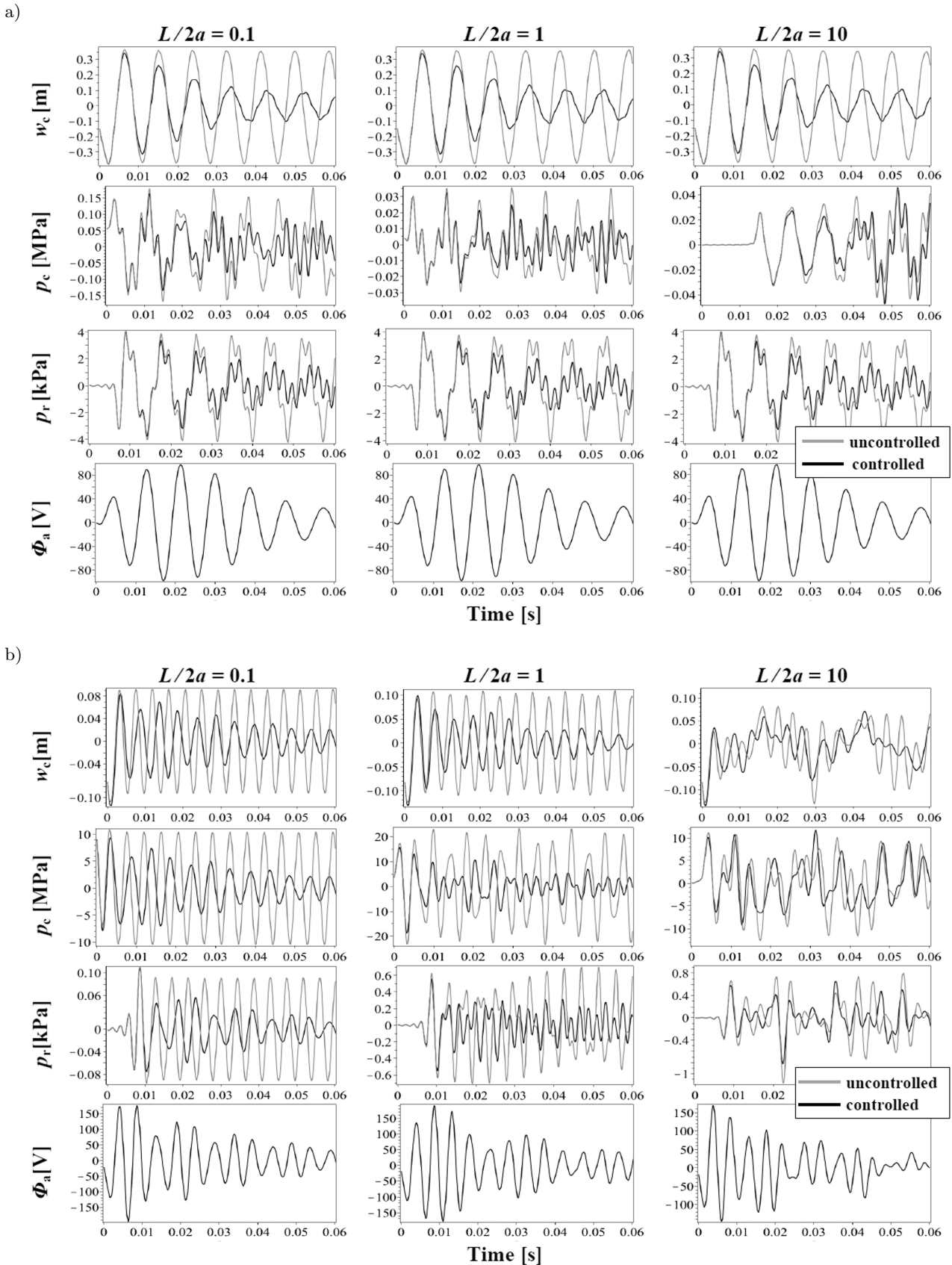
Fig. 3. The uncontrolled and controlled time histories of transverse panel center-point displacement, cavity center-point sound pressure, on-axis external radiated acoustic pressure, and applied control voltage, due to an impulsive central transverse point load, for selected internal cavity fluids and depth parameters: a) air-filled cavity, b) water-filled cavity.
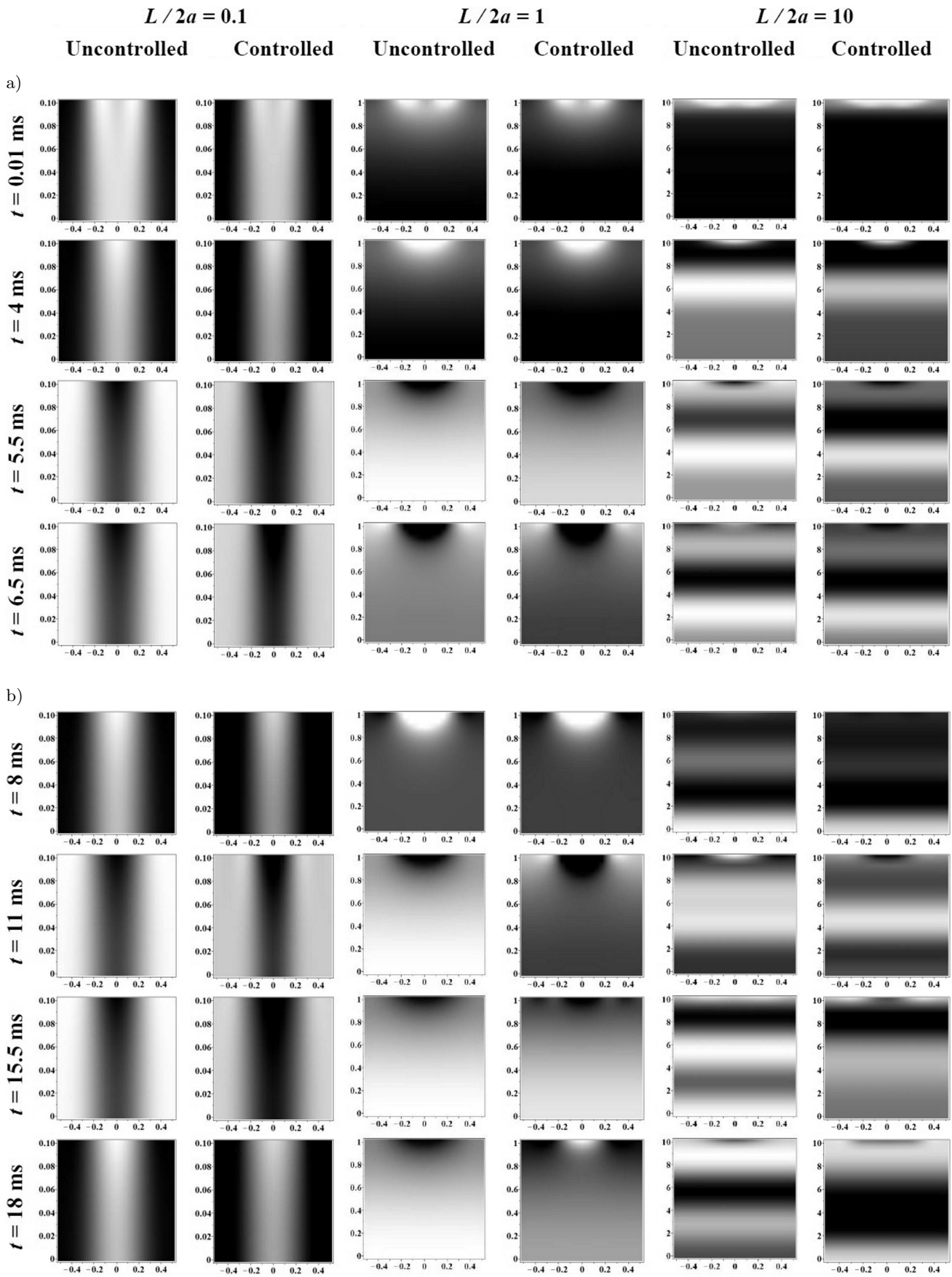
Fig. 4. Time-domain snapshots of the uncontrolled and controlled (water-filled) cavity sound pressure field, due to an impulsive central transverse point load, for selected cavity depth parameters.

readily be made. In particular, the overall effectiveness of control action for short and medium size cavities in moderate to late-times (as signified by larger dark areas) is evident in the 2D images. The most interesting distinction is perhaps the effect of active damping control (ADC) action on the distribution (propagation) of sound pressure energy within the piezo-panel-coupled cylindrical enclosure. In particular, the radiated impulsive wave fronts appear to travel horizontally (i.e., reverberate in the radial direction) within the shortest cavity ($L/2a = 0.1$), while they nearly travel along the cavity axis (i.e., towards the cavity bottom) in the long cavity situation ($L/2a = 10$). For cavity of intermediate depth ($L/2a = 1$), the wave forms behave somewhat in between the other two configuration (i.e., the spherical impulsive waves radiate from the lower surface of composite panel into the cylindrical enclosure).

4. Conclusions

The 3D non-axisymmetric non-stationary active sound radiation and vibration control of a thin trilaminate piezo-composite circular panel coupled to a backing hard-walled cylindrical enclosure of finite depth, while driven by general distributed transverse impulsive mechanical surface loads, has been investigated rigorously. The smart structure consisted of a supporting core isotropic layer perfectly bonded to transversely polarized lower/upper piezoelectric sensor/actuator skin layers. Active damping is achieved through a GA-tuned proportional control law with a multi-objective cost function, where the induced sensor voltage is directly fed back into the piezo-actuator layer. Durbin's numerical inverse Laplace transform scheme is exploited to calculate the time evolutions of key acousto-structural parameters and the actuator (control) voltage. It is found that a substantial increase in the water-filled cavity depth causes notable modification of the output acousto-structural variables, while the depth of the air-filled cavity has negligible effect on the panel displacement and the resulting radiated external pressure field, largely due to presence of light fluid loading. Also, effectiveness of the adopted distributed active damping control configuration in adequate mitigation of panel displacement and external radiated sound pressure field is established, especially for cylindrical enclosures of shallow and moderate depths, almost regardless of cavity inner fluid type. In addition, control authority on the internal sound field is seen to progressively deteriorate as the cavity depth increases, especially for the water-filled cavity. Moreover, the effect of cavity depth on the control voltage is not very prominent, while the required actuator voltage levels nearly double as the internal cavity fluid is changed from air to water (i.e., higher actuation power required

for heavier fluid loading). The presented results can be useful for analyses of the transient fluid-structure interaction control of panel components coupled to cylindrical enclosures, including a number of visualization methods and computer programs. Furthermore, the offered set of precise space-time converged solutions can provide expedient data for structural acoustic designers/engineers, as a canonical benchmark for confirmation of other solutions attained by largely restrictive asymptotic or numerical procedures.

Appendix

This Appendix contains the definitions of some key parameters used in the "Structural model" Subsec. 2.2. In particular, the piezoelectric material constants (C_{11}, C_{12}, e_{31}) appearing in the stress-displacement relations (7) are defined as:

$$C_{11} = \overline{c}_{11} - \left(\frac{\overline{c}_{11}}{\overline{c}_{33}}\right)^2,$$

$$C_{12} = \overline{c}_{12} - \left(\frac{\overline{c}_{13}}{\overline{c}_{33}}\right)^2,$$

$$e_{31} = \overline{e}_{31} - \frac{\overline{c}_{13}\overline{e}_{33}}{\overline{c}_{33}},$$

where $\overline{c}_{ij}$ are the elastic moduli, $\overline{e}_{ij}$ are the piezoelectric constants, and E_{11} and E_{33} are the dielectric constants of the piezoelectric (PZT4) material (see Table 1). Also, the total electric field components (E_r, E_θ, E_z) appearing in the stress-displacement relations (7) are defined in terms of relevant electric potentials as (WANG *et al.*, 2001):

$$E_r = -\frac{\partial \Phi}{\partial r} = -\frac{1}{h_1^3}(z-h-h_1)(z^2-h^2)\frac{\partial \Phi_s}{\partial r}$$
$$\quad -\frac{1}{h_1^3}(z+h+h_1)(z^2-h^2)\frac{\partial \Phi_a}{\partial r},$$

$$E_\theta = -\frac{1}{r}\frac{\partial \Phi}{\partial \theta} = -\frac{1}{h_1^3}(z-h-h_1)(z^2-h^2)\frac{1}{r}\frac{\partial \Phi_s}{\partial \theta}$$
$$\quad -\frac{1}{h_1^3}(z+h+h_1)(z^2-h^2)\frac{1}{r}\frac{\partial \Phi_a}{\partial \theta}, \quad (30)$$

$$E_z = -\frac{\partial \Phi}{\partial z} = -\frac{1}{h_1^3}\left[(z^2-h^2)+2z(z-h-h_1)\right]\Phi_s$$
$$\quad -\frac{1}{h_1^3}\left[(z^2-h^2)+2z(z+h+h_1)\right]\Phi_a.$$

Furthermore, the associated electric displacement components (D_r, D_θ, D_z) that are substituted into the classical Maxwell equation (13) are written as:

$$D_r = \Xi_{11}E_r = -\frac{\Xi_{11}}{h_1^3}(z-h-h_1)(z^2-h^2)\frac{\partial \Phi_s}{\partial r}$$
$$-\frac{\Xi_{11}}{h_1^3}(z+h+h_1)(z^2-h^2)\frac{\partial \Phi_a}{\partial r},$$

$$D_\theta = \Xi_{11}E_\theta = -\frac{\Xi_{11}}{h_1^3}(z-h-h_1)(z^2-h^2)\frac{1}{r}\frac{\partial \Phi_s}{\partial \theta}$$
$$-\frac{\Xi_{11}}{h_1^3}(z+h+h_1)(z^2-h^2)\frac{1}{r}\frac{\partial \Phi_a}{\partial \theta}, \quad (31)$$

$$D_z = \Xi_{33}E_z + e_{31}\left(\frac{\partial u_r}{\partial r} + \frac{\partial u_\theta}{r\partial \theta} + \frac{u_r}{r}\right)$$
$$= -\frac{\Xi_{33}}{h_1^3}\left[(z^2-h^2) + 2z(z-h-h_1)\right]\Phi_s$$
$$-\frac{\Xi_{33}}{h_1^3}\left[(z^2-h^2) + 2z(z+h+h_1)\right]\Phi_a - e_{31}z\Delta w,$$

where $\Xi_{11} = E_{11}$, and $\Xi_{33} = E_{33} + \overline{e}_{33}^2/\overline{c}_{33}$. Moreover, the resultant piezo-coupled moments $(M_{rr}, M_{\theta\theta}, M_{r\theta})$ appearing in the shear force relations (9) are expressed as (WANG *et al.*, 2001):

$$M_{rr} = \int_{-h}^{h} z\sigma_{rr}\,\mathrm{d}z + 2\int_{h}^{h+h_1} z\Sigma_{rr}\,\mathrm{d}z$$
$$= -\left[(D_1+D_2)\frac{\partial^2 w}{\partial r^2} + \left(\nu D_1 + \frac{C_{12}}{C_{11}}D_2\right)\right.$$
$$\left.\cdot\left(\frac{1}{r}\frac{\partial w}{\partial r} + \frac{1}{r^2}\frac{\partial^2 w}{\partial \theta^2}\right) - D_3 e_{31}\Phi_s - D_4 e_{31}\Phi_a\right],$$

$$M_{\theta\theta} = \int_{-h}^{h} z\sigma_{\theta\theta}\,\mathrm{d}z + 2\int_{h}^{h+h_1} z\Sigma_{\theta\theta}\,\mathrm{d}z$$
$$= -\left[\left(\nu D_1 + \frac{C_{12}}{C_{11}}D_2\right)\frac{\partial^2 w}{\partial r^2} + (D_1+D_2)\right. \quad (32)$$
$$\left.\cdot\left(\frac{1}{r}\frac{\partial w}{\partial r} + \frac{1}{r^2}\frac{\partial^2 w}{\partial \theta^2}\right) - D_3 e_{31}\Phi_s - D_4 e_{31}\Phi_a\right],$$

$$M_{r\theta} = \int_{-h}^{h} z\sigma_{r\theta}\,\mathrm{d}z + 2\int_{h}^{h+h_1} z\Sigma_{r\theta}\,\mathrm{d}z$$
$$= -\left[(1-\nu)D_1 + \left(1-\frac{C_{12}}{C_{11}}\right)D_2\right]$$
$$\cdot\left(\frac{1}{r}\frac{\partial^2 w}{\partial r\partial \theta} - \frac{1}{r^2}\frac{\partial w}{\partial \theta}\right),$$

where

$$D_1 = \frac{2Eh^3}{3(1-\nu^2)},$$
$$D_2 = \frac{2}{3}h_1\left(3h^2 + 3hh_1 + h_1^2\right)C_{11},$$
$$D_3 = \left(\frac{2}{3}h + \frac{1}{6}h_1\right),$$
$$D_4 = \frac{1}{6h_1^2}\left(48h^3 + 96h^2h_1 + 68hh_1^2 + 17h_1^3\right).$$

References

1. ABAQUS, Analysis User's Manual Version 6.11 Online Documentation.

2. ABRAMOWITZ M., STEGUN I. (1964), *Handbook of Mathematical Functions with Formulas, Graphs, and Mathematical Tables*, 3rd ed, New York: National Bureau of Standards.

3. AL-BASSYIOUNI M., BALACHANDRAN B. (2005), *Sound transmission through a flexible plate into an enclosure: structural-acoustics model*, Journal of Sound and Vibrations, **284**, 467–486.

4. AZZOUZ M.S., RO J. (2002), *Control of sound radiation of an active constrained layer damping plate/cavity system using the structural intensity approach*, Journal of Vibration and Control, **8**, 903–918.

5. BALACHANDRAN B., SAMPATH A. (1996), *Active control of interior noise in a three-dimensional enclosure*, Smart Materials and Structures, **5**, 89–97.

6. CARESTA M., KESSISSOGLOU N.J. (2010), *Acoustic signature of a submarine hull under harmonic excitation*, Applied Acoustics, **71**, 17–31.

7. CASADEI F., DOZIO L., RUZZENE M., CUNEFARE K.A. (2010), *Periodic shunted arrays for the control of noise radiation in an enclosure*, Journal of Sound and Vibrations, **329**, 3632–3646.

8. CHENG L., NICOLAS J. (1992), *Radiation of sound into a cylindrical enclosure from a point driven end plate with general boundary conditions*, Journal of Acoustical Society of America, **91**, 1504–1513.

9. COMRIE J.L., KORDE U.A. (2012), *Vibroacoustic studies on sounding rocket bulkheads*, Proceedings of SPIE – The International Society for Optical Engineering, **8341**, 17–33.

10. Duan W.H., Quek S.T., Wang Q. (2005), *Free vibration analysis of piezoelectric coupled thin and thick annular plate*, Journal of Sound and Vibrations, **281**, 119–139.

11. DURBIN F. (1973), *Numerical inversion of Laplace transforms: an effective improvement of Dubner and Abate's method*, Computer Journal, **17**, 371–376.

12. FULLER C.R. (1990), *Active control of sound transmission/radiation from elastic plates by vibration inputs, I-analysis*, Journal of Sound and Vibrations, **136**, 1–15.

13. Genetic Algorithm Toolbox Available, http://www.mathworks.com/products/global-optimization/description4.html.

14. GORMAN D.G., REESE J.M., HORACEK J., DEDOUCH K. (2001), *Vibration analysis of a circular disc backed by a cylindrical cavity*, Proceedings of the Institution of Mechanical Engineers, Part C: Journal of Mechanical Engineering Science, **215**, 1303–1311.

15. GORMAN D.G., TRENDAFILOVA I., MULHOLLAND A.J., HORACEK J. (2008), *Vibration analysis of a circular plate in interaction with an acoustic cavity leading to extraction of structural modal parameters*, Thin walled Structures, **46**, 878–886.

16. HASHEMINEJAD S.M., SHAKERI R., REZAEI S. (2012), *Vibro-acoustic response of an elliptical plate-cavity coupled system to external shock loads*, Applied Acoustics, **73**, 757–769.

17. HASHEMINEJAD S.M., ALAEI-VARNOSFADERANI M. (2012), *Vibroacoustic response and active control of a fluid-filled functionally graded piezoelectric material composite cylinder*, Journal of Intelligent Materials Systems and Structures, **23**, 775–790.

18. HASHEMINEJAD S.M., KESHAVARZPOUR H. (2013), *Active sound radiation control of a thick piezolaminated smart rectangular plate*, Journal of Sound and Vibrations, **332**, 4798–4816.

19. HASHEMINEJAD S.M., RABBANI V. (2015), *Active damping of transient sound radiation from a smart piezocomposite hollow cylinder*, Archives of Acoustics, **40**, 359–381.

20. JIN G., LIU X., LIU Z., YANG T. (2011), *Active control of structurally radiated sound from an elastic cylindrical shell*, Journal of Marine Science and Application, **10**, 88–97.

21. JUNGER M.C, FEIT D. (1986), *Sound, Structures and Their Interaction*, 3rd ed, Cambridge: MIT Press.

22. KIM J., KO B., LEE J.K., CHEONG C.C. (1999), *Finite element modeling of a piezoelectric smart structure for the cabin noise problem*, Smart Materials and Structures, **8**, 380–389.

23. KOSHIGOE S., MURDOCK J.W. (1993), *A new approach for active control of sound transmission through an elastic plate backed by a rectangular cavity*, Journal of Acoustical Society of America, **94**, 900–907.

24. NASHIF A.D., JONES D.I.G., HENDERSON J.P. (1986), *Vibration Damping*, New York: Wiley.

25. NIEKERK J.L., TONGUE B.H. (1997), *On the active control of transient noise transmission*, Applied Acoustics, **50**, 1–22.

26. NIEZRECKI C., CUDNEY H.H. (2001), *Feasibility to control launch vehicle internal acoustic using piezoelectric actuators*, Journal of Intelligent Material Systems and Structures, **12**, 647–660.

27. PAN J., HANSEN C.H. (1991), *Active control of noise transmission through a panel into a cavity III: Effect of the actuator location*, Journal of Acoustical Society of America, **90**, 1493–1501.

28. RAO S.S. (2007), *Vibration of Continuous Systems*, New York: Wiley.

29. RAY M.C., REDDY J.N. (2004), *Performance of piezoelectric fiber reinforced composites for active structural-acoustic control of laminated composite plates*, IEEE Transactions Ultrasonics Ferroelectrics and Frequency Control, **51**, 1477–1490.

30. RAY M.C., FAYE A., PATRA S., BHATTACHARYYA R. (2009), *Theoretical and experimental investigations on the active structural-acoustic control of a thin plate using a vertically reinforced 1–3 piezoelectric composite*, Smart Materials and Structures, **18**, 1–13.

31. RO J., BAZ A. (1999), *Control of sound radiation from a plate into an acoustic cavity using active constrained layer damping*, Smart Materials and Structures, **8**, 292–300.

32. SAMPATH A., BALACHANDRAN B. (1999), *Active control of multiple tones in an enclosure*, Journal of Acoustical Society of America, **106**, 211–225.

33. SHAKERI R., YOUNESIAN D. (2015), *Broad-band noise mitigation in vibrating annular plates by dynamic absorbers*, International Journal of Structural Stability and Dynamics, **16**, 1–30.

34. SHIELDS W., RO J., BAZ A. (1998), *Control of sound radiation from a plate into an acoustic cavity using active piezoelectric-damping composites*, Smart Materials and Structures, **7**, 1–11.

35. VEERAMANI S., WERELEY N.M. (1996), *Hybrid passive/active damping for robust multivariable acoustic control in composite plates*, Proceeding SPIESymp Smart Materials and Structures, 374–387.

36. VEL S.S., BAILLARGEON B.P. (2005), *Analysis of static deformation vibration and active damping of cylindrical composite shells with piezoelectric shear actuators*, Journal of Vibration and Acoustics, **127**, 395–407.

37. WANG Q., QUEK S.T., SUN C.T., LIU X. (2001), *Analysis of piezoelectric coupled circular plate*, Smart Materials and Structures, **10**, 229–39.

38. YANG X., LANG J.H., SLOCUM A.H. (2007), *Circular plate electrostatic zipping actuator for the application of a tunable electromagnetic cavity resonator*, IEEE, 655–658.